

In Situ Reconnection of Nanoelectrodes Over 20 nm Gaps on Polyimide Substrate

Xubin Zhang, Zhibin Zhao, Surong Zhang, Adila Adijiang, Tianran Zhao, Min Tan, Xueyan Zhao, Qihong Hu, Maoning Wang, Takhee Lee, Elke Scheer,* and Dong Xiang*

The current densities in nowadays electronic circuitry are close to the electromigration threshold that may result in the fracture of circuits due to electromigration, hampering further miniaturization of integrated chips. Flexible electronic devices, which use a flexible material instead of rigid silicon as a substrate, might be prone to fracture problems also due to obligatory mechanical deformation. However, finding the location of fractured nanogaps and in situ repairing such atomic-scale fractured circuits are currently unavailable. To this end, a method is developed to in situ heal nanogaps as large as 20 nm between metallic electrodes on the polyimide (PI)-covered substrate *via* voltage sweeping, which is typically employed to generate nanogaps rather than heal nanogaps. The reconnection of nanoelectrodes is realized only when the underneath PI is treated with oxygen plasma etching. Assisted by X-ray photoelectron spectroscopy, it is revealed that inductively coupled O₂ plasma etching not only changes the surface topography but also changes the chemical binding structure of PI, which in return can be used to immobilize metal atoms migrating along the PI surface to gradually close the nanogap, providing an in situ self-healing paradigm for repairing the atomic scale fractured circuits.


approaching the electromigration threshold which may “burn” the smallest constriction of the circuit and hence result in the failure of circuits.^[3–6] On the other hand, for functionalized electronic devices based on flexible substrates,^[7–10] mechanical deformation also leads to the breakage of nanoelectronic circuits.^[11,12] Therefore, it is highly desired to reconnect such fractured electrodes to reestablish the function of the electronic devices. However, repairing such atomic scale fractured circuits in situ faces great challenges by traditional methods (e.g., welding),^[13–16] because atomic scale gaps are quite difficult to be addressed by welding, and the whole chip may be completely destroyed by the heating of soldering. Local deposition of conductive material using a focused ion beam and dielectrophoresis might be successfully used,^[17–19] but are incapable of being applied after packaging.

To this end, we put forward a straightforward approach to in situ reconnect the gaps on the flexible polyimide (PI)-covered substrate by voltage sweeping and metal atom trapping, i.e., *via* trapping the metal atoms migrating along the PI surface driven by electromigration. The concept of electromigration has been considered as a failure mode in microelectronic circuitry for a long time due to that it causes the breakdown of circuitry.^[6] Previous study further demonstrated that cracks formed due to electromigration can disappear upon the

1. Introduction

Continuously shrinking the size of components in electronic circuits is critically important to follow Moore’s Law.^[1] Although modern fabrication techniques have reduced the lateral feature size in the circuits down to nanometers, further miniaturizing functional electronic circuits still meets great challenges.^[2] One of the challenges is that the current density in circuits is

X. Zhang, Z. Zhao, S. Zhang, A. Adijiang, T. Zhao, M. Tan, X. Zhao, Q. Hu, M. Wang, D. Xiang
Institute of Modern Optics and Center of Single-Molecule Science
Tianjin Key Laboratory of Micro-scale Optical Information Science and Technology
Nankai University
Tianjin 300350, China
E-mail: 015008@nankai.edu.cn

 The ORCID identification number(s) for the author(s) of this article can be found under <https://doi.org/10.1002/ssr.202300283>.

© 2023 The Authors. Small Structures published by Wiley-VCH GmbH. This is an open access article under the terms of the Creative Commons Attribution License, which permits use, distribution and reproduction in any medium, provided the original work is properly cited.

DOI: 10.1002/ssr.202300283

M. Wang, E. Scheer
Department of Physics
University of Konstanz
78457 Konstanz, Germany
E-mail: elke.scheer@uni-konstanz.de

T. Lee
Department of Physics and Astronomy, and Institute of Applied Physics
Seoul National University
Seoul 08826, Korea

D. Xiang
School of Materials Science and Engineering
Smart Sensing Interdisciplinary Science Center
Nankai University
Tianjin 300350, China

application of a high-density current at the right duration and the closure of the cracks result from the electro-migrative mass diffusion.^[20,21] Here, we show that electromigration combined with atom trapping can be employed to heal (to close) the nanogap in a more controllable manner. Two types of nanogaps on PI substrates were prefabricated in our experiments: one is fabricated by direct electron beam lithography (EBL), and the other one is fabricated by burning a nano-constriction *via* local current heating. We found that both types of nanogaps (even larger than 20 nm) can be reconnected by performing voltage sweeps if the substrates had been pretreated by O₂-contained plasma etching. In contrast, the reconnection of electrodes was not observed regardless of the gap sizes (even as small as 5 nm) if the substrate was not pretreated by plasma etching. The underlying mechanism for the interesting observation is proposed, showing a route for self-healing nanoscale circuits in case of that they are not embedded in an insulator.

2. Results and Discussion

A gold nanoelectrode pair on a PI layer above a silicon wafer was prefabricated by a standard process of EBL, see Figure S1 and S2 (Supporting Information) for detailed information. PI is routinely used as bulk substrate material for flexible electronics and also as a cover layer to provide electrical isolation to other substrate materials.^[22,23] **Figure 1** shows the electrical characterization of the sample employing an unetched PI substrate with an initial nanogap of ≈ 5 nm. Figure 1a is the scheme of the

electrical circuit, showing that a tunable voltage is applied to the electrode pair, see Figure S3 (Supporting Information) for detailed information. Figure 1b,c shows the scanning electron microscope (SEM) images of the sample before and after dozens of voltage sweeps. It can be found that the initial gap (≈ 5 nm) of the sample has been enlarged (≈ 20 nm) after voltage sweeps in a large range (up to ± 8 V). With a close examination of the SEM image, it can be found that a part of the sharp tip of the left electrode is removed from the electrode, resulting in the enlargement of the gap size. The removal of atoms from the electrode tip is also observed for other samples when the voltage sweeps range is enlarged, see Figure S4 (Supporting Information). We attribute the enlargement of the gap size to metal atom migration driven by the electric field^[14,24–26] and the field emission current,^[27,28] which strongly depends on the curvature of the electrode. We will discuss this point in more detail later.

Figure 1d–f depicts the current–voltage (*I*–*V*) curves of the sample under different small voltage ranges. Asymmetric *I*–*V* curves were observed. The measured current at the level of dozens of μ A is assigned to the field emission current caused by the electric field concentrated at the electrode tip.^[27,28] The measured current at level of dozens of μ A with asymmetric *I*–*V* curves is assigned to the field emission current caused by the electric field concentrated at the electrode tip rather than the tunneling current through air or PI based on the factors: 1) the tunneling current should be quite small far below μ A with a gap size of ≈ 5 nm since the tunneling current exponentially decreases with the increase of the gap size^[29]; 2) the tunneling *I*–*V* curves of a nanogap typically show a symmetric shape since it is independent of

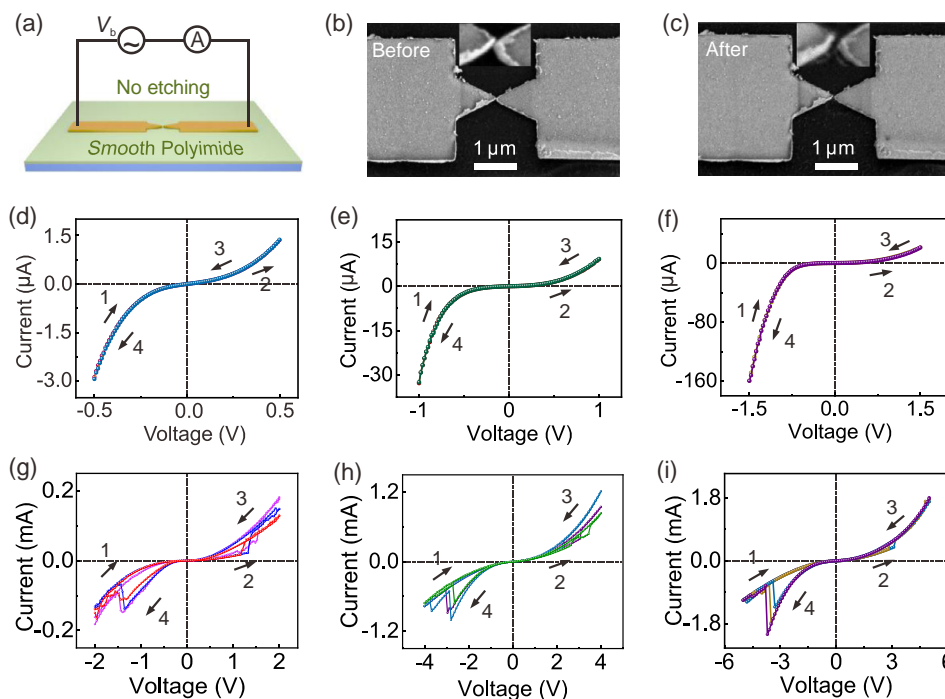


Figure 1. *I*–*V* characterization and SEM images of the sample using unetched PI as substrate. a) Schematic diagram of the electrical measurement employing unetched PI. b) SEM image of the sample before the voltage sweeps and c) after dozens of voltages sweep up to $(-8, 8)$ V. The gap size was enlarged from ≈ 5 to ≈ 20 nm after voltage sweeps. d–f) The *I*–*V* curves of the junction within a small voltage range. The numbers show the time order within one voltage sweep. g–i) The *I*–*V* curves of the junction when the voltage sweep range was enlarged. Reproducible conductance switching was observed.

the topography of the electrodes^[30]; and 3) the field emission I - V curves will show asymmetric shape once the curvatures of two electrode tips are different.

Notably, no current jump and no hysteretic behavior are observed even if the voltage range is enlarged to ± 1.5 V. However, as the voltage sweeping range was further increased to ± 2.0 V, a reproducible conductance switching phenomenon was observed as shown in Figure 1g-i. This switching was accompanied by a symmetric shape in the I - V curves, i.e., the asymmetric I - V curves become symmetric after switching, as demonstrated in Figure S5 (Supporting Information). Moreover, it was observed that the trigger voltage for the switching shifted to a higher value as the voltage sweeping window was expanded. Upon further enlarging the sweep range to ± 8 V, the I - V curves became unstable and unreproducible. The mechanism for the switch phenomenon will be addressed later. Here, we point out that the I - V curves never show linear ohmic behavior, indicating that the two electrodes do not connect even upon a high voltage bias. The disconnection of two electrodes was also observed for other samples on the unetched PI with a gap size of ≈ 25 nm and ≈ 15 nm after dozens of voltage sweeps, see Figure S6 (Supporting Information).

We further fabricated an electrode pair above PI with a gap size of ≈ 20 nm, and then the PI surface was treated by inductively coupled plasma (ICP) etching using O_2 gas and CHF_3 . The unprotected PI layer (≈ 200 nm in thickness) was removed during the etching process, see Figure S1 (Supporting Information) for detailed information. Figure 2a presents a schematic diagram of the electrical circuit. Figure 2b shows a symmetric S-shaped I - V curve in the voltage range -0.4 to 0.4 V.

Figure 2c shows that the symmetric I - V curves transform into asymmetric I - V curves when the voltage sweep range is enlarged to ± 1.0 V. Simultaneously, a pronounced hysteretic behavior becomes evident, and the whole negative current level gradually increases with repeated voltage sweeps, as shown in Figure 2d. The gradually increased current and pronounced hysteretic behavior indicate that the properties of PI inside the gap and/or the geometry of the electrodes are gradually changed upon repetition of the voltage sweeps.^[15]

Interestingly, the current suddenly jumps to a high level from ≈ -0.5 μ A to ≈ -1.6 mA at $V \approx 1.2$ V after approximately 20 voltage sweeps (Figure 2e), and then the I - V curve shows a linear shape (Figure 2f), i.e., presents ohmic behavior, signaling that a direct metallic contact has formed. The conductance of the circuit is calculated to be $G \approx 610$ μ S $\gg 1$ G_0 , confirming that the two electrodes are connected after the current jump, where $G_0 = 2e^2/h \approx 77$ μ S is the conductance quantum. The I - V curves present linear characterization and show high reproducibility when the sweep window is enlarged to $[-0.6, 0.6$ V], indicating that the nanogap is stably reconnected by Au atoms. It can be predicted that the stability of the healed nanogap will be enhanced when the electrodes (metal atoms) are buried by other materials or covered by other materials during the encapsulation process since the surrounding material will restrain the migration of Au atoms. To identify what happened during the I - V sweeping process, we took a series of SEM images of the sample before and after I - V sweeping.

Figure 2g shows an SEM image of the sample before voltage sweeps, and Figure 2h shows an SEM image of the sample after

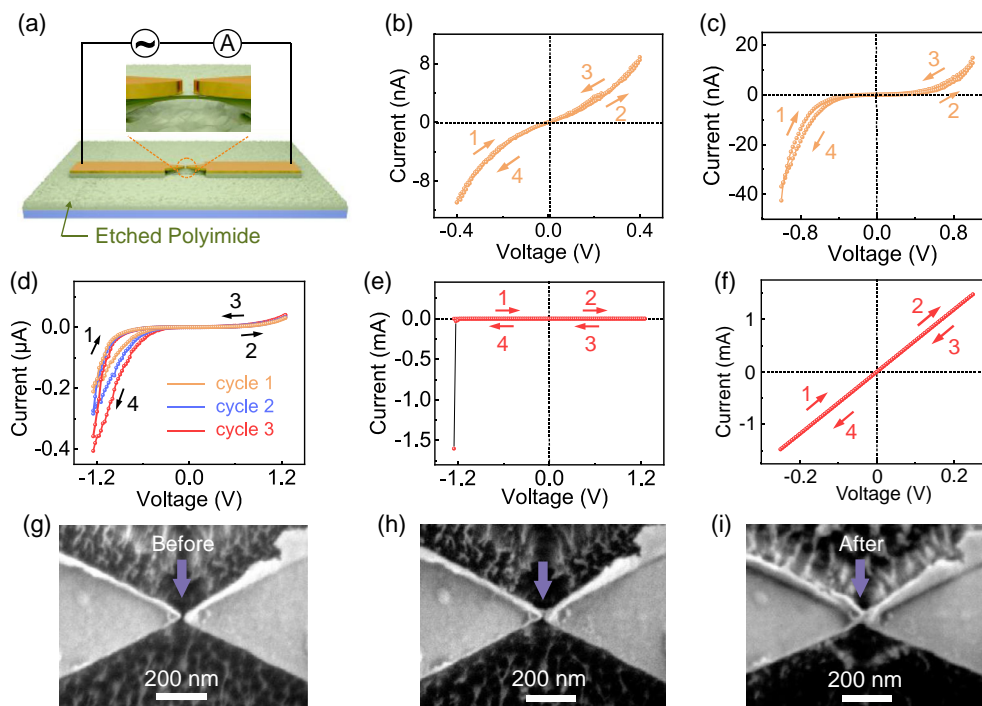


Figure 2. Connection of the nanoelectrodes over 20 nm gap on the etched PI. a) Schematic diagram of the sample and the electrical measurement circuit. The insert shows a pair of suspended electrodes connected with a PI film underneath the electrodes. b-f) I - V curves of the junctions at different bias voltage ranges. The arrows/numbers indicate the direction/time order within one voltage sweep. g) SEM image of the investigated sample before I - V sweeping. h) SEM image of the sample after repetition of 20 voltage sweeps. i) SEM image of the sample after a further repetition of 20 voltage sweeps.

about 20 voltage sweeps (i.e., after the conductance jump). It can be clearly seen that the morphology of the electrode near the gap drastically changed, and the bottom of the two electrodes seem to be bridged by some material after voltage sweeping, see Figure S7 (Supporting Information) for detailed analysis. Figure 2i shows that the nanogap between two electrodes was further filled by some materials upon further voltage sweeps. Based on the observation that the I - V curves present a metallic linear shape, we claim that this bridging material should be an electric conductor. To test the reliability of the voltage-driven-connection approach, we further fabricated the second type of nanogap by burning the constriction and tried to reconnect them. Interestingly, it is observed that two separated electrodes can be reconnected even though the gap size is much larger than 20 nm, see Figure S8 (Supporting Information) for detailed information.

Comparing Figure 1 and 2, it becomes evident that the surface characteristics of the PI substrate, altered through plasma etching, play a crucial role in the connection of the nanoelectrodes. It has been reported that oxygen-argon plasma pretreatment not only increases the roughness of the PI surface but also changes its chemical binding structure.^[31] In more detail, O_2 plasma etching makes the smooth surface of PI rough by generating a grass-shaped topography^[32] and significantly increases the amount of O_2 -containing functional groups such as carboxyl ($-COO$), carbonyl ($=CO$), ether ($-CO$), and hydroxyl (OH) groups due to

chain scission.^[33,34] Fourier transform infrared spectroscopy analysis has proven that C–O bonds were generated after the O_2 plasma treatment.^[35] X-ray photoelectron spectroscopy (XPS) and high-resolution electron energy loss spectroscopy have shown that evaporated Al reacts preferentially with C–O groups to form C–O–Al complexes due to their high reactivity.^[36–38] We conjecture that a similar mechanism may be at play here as well, although the chemical reactivity of Al and Au is different. Meanwhile, in situ generation of C–Au covalent contacts has also been reported under certain conditions.^[39,40] Therefore, we assume the terminal functional groups generated by the O_2 -plasma etching result in the distinguished behavior of the etched PI compared to the unetched PI.

Figure 3a shows the synthesis route of the PI used in our experiments. The poly (amic acid) (PAA, precursor of PI) was mass produced by polymerizing pyromellitic dianhydride (PMDA) with 4,4'-oxydianiline.^[41] Then, the PAA was imidized into PI films ($\approx 75\%$) by curing them at $200^\circ C$ in ambient conditions for cross-linking.^[42,43] The oxygen ion will attack the imide ring ($O=C-N-C=O$) in the plasma etching process, making the carbonyl ($C=O$) change into the carboxyl group with a terminal C–O group.^[35]

To identify what had been changed during the etching process, XPS was performed to analyze the chemical composition of the PI surface by measuring the binding energy of C 1s, N

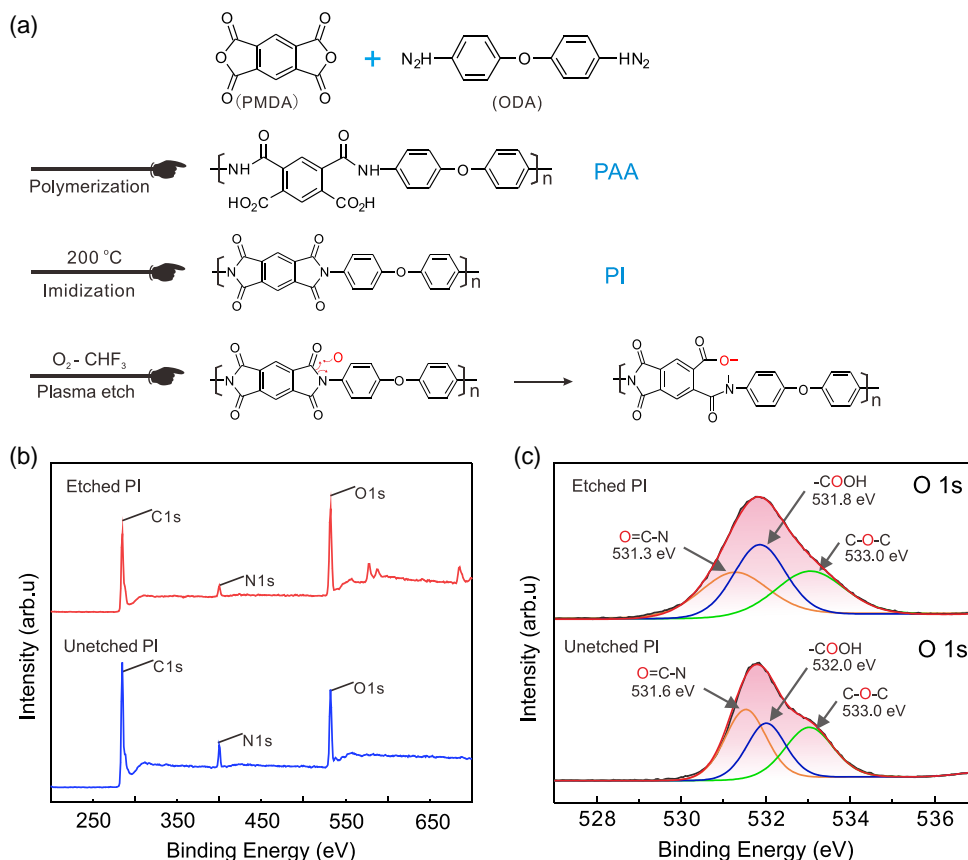


Figure 3. Synthetic route to PAA and PI, and XPS of polyimide (PMDA-ODA). a) Synthetic route to prepare PAA and PI. Mechanism of O_2 plasma reaction at the PI surface. b) XPS spectra of the PI before and after etching showing the C 1s, N 1s, and O 1s peaks. c) Zoomed O 1s XPS spectra of the etched and unetched PI.

1s, and O 1s of PI, as presented in Figure 3b. The ratio of the O/C intensities for etched PI increased significantly compared to the one of unetched PI, which indicates that O₂-containing groups were introduced during O₂ plasma etching. The O 1s XPS spectra of PI are shown in Figure 3c, and the C 1s XPS spectra of PI are shown in Figure S9 (Supporting Information). The peaks centered at 531.3 eV in etched PI and 531.6 eV in unetched PI are assigned to the imide groups (O=C-N), and the peaks centered at 531.8 eV in etched PI and 532.0 eV in unetched PI are assigned to carboxylic acid groups (COOH).^[44] The peak located at 533.0 eV was attributed to the C-O-C group in the cyclic anhydride.^[43,45]

We find that the peak height of O=C-N of the etched PI is lower than the one of the unetched PI, indicating a ring-opening reaction of the imide groups. Meanwhile, the peak height of -COOH in the etched PI is higher than the one in the unetched PI, indicating the carbonyl group is changed into the carboxylic acid group (COO⁻) with a terminal C-O bond,^[35] as presented in Figure 3a. The resulting C-O bond can serve as a reaction site to increase the adhesion between the gold atoms and PI by forming a C-O-Au bond.^[31,35]

The earlier findings shed light on the mechanism of junction' conductance switching on the unetched PI and reconnection of the electrodes on the etched PI, as presented in Figure 4. Figure 4a-c shows the schematic of conductance switch mechanism above the unetched PI. Due to the short distance between the two electrodes (a few nanometers) and the sharp shape of electrodes, the electric field may be sufficiently strong to induce a field emission current even at low bias voltages.^[46] Driven by the electric field, certain atoms may migrate toward the electrode tip, resulting in the formation of an even sharper tip with atomic-scale curvature. Correspondingly, the movement of gold atoms toward the tip will lead to an increase in the field emission current, as illustrated in Figure 4b. Conversely, when the bias voltage is reversed, the gold atoms at the tip undergo rearrangement, potentially causing the atomic sharp tip to become blunter, as shown in Figure 4c. This process subsequently leads to a

decrease in the current. During the voltage sweeping process, the polarity of the bias voltage is periodically changed that results in reversible conductance switching, see Figure S10 (Supporting Information) for detailed analysis. The rearrangement of the atoms always makes two electrodes have similar curvature. Therefore, the *I-V* curves after atom rearrangement (conductance switching) become more symmetric. Please note that with a further increase in the applied bias voltage, the movement of gold atoms might become violent, and these atoms might migrate away from the electrode surface which will result in the enlargement of the gap size, as previously demonstrated in Figure 1b,c.

In contrast, the connection of two gold electrodes on the etched PI substrates can be schematically explained by Figure 4d-f. Excited by the electric field and field emission current, the gold atoms may escape from the electrode surface,^[14,24-27] migrating along the PI surface toward the opposite electrode. In contrast to the pristine PI with a quite smooth surface, the ICP etched PI has a quite rough surface which will reduce the mobility of gold atoms on the PI surface, as shown in Figure 4d. Meanwhile, many active reaction sites generated during the O₂ plasmonic etching process will greatly improve the adhesion between the metal atoms and the PI by forming C-O-Au bonds.^[35] In other words, these migrating atoms have the opportunity to be trapped by -COO⁻ groups, forming metal atom complexes,^[47-49] as schematically shown in Figure 4e. The accumulation of metal atoms within the gap leads to an increase in current (as well as hysteretic behavior) and ultimately results in the connection of the initially gapped electrodes, as shown in Figure 4f. In contrast, the smooth surface and absence of bonding groups of unetched PI make it difficult to trap migrated gold atoms. Consequently, connecting the two electrodes using unetched PI becomes highly challenging due to the lack of a precursor for atom accumulation within the nanogap.

To confirm that the reconnection of electrodes truly originates from metal atoms migrating and trapping along the PI surface, we further fabricated a vertical stacked gold-PI-gold junction, in

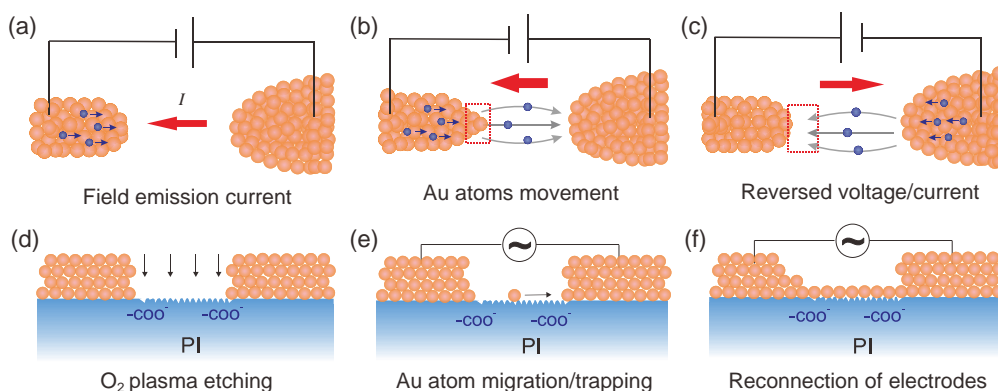


Figure 4. Schematic diagram of atoms rearrangement at the electrode surface and atoms migration along the etched PI surface. a-c) Plan view of the surface morphologies of the electrodes on the unetched PI under the action of field emission current. The red arrows indicate the direction of the current. The blue balls and gray arrows indicate the electrons and their moving directions, respectively. d-f) Side view of the reconnection process of two electrodes. d) The O₂ ions attack the backbone of the PI molecular chain to break imide bonds and form new bonds (e.g., -COO⁻) in the O₂ plasma etching process. A rough surface is generated during the etching process. e) The process of gold atoms migrating along the PI surface upon a voltage sweep. The migrated metal atom may be trapped by the etched PI serving as a precursor for the atom accumulation. f) The accumulation of metal atoms results in the reconnection of nanoelectrodes.

which the two gold layers are completely insulated by the PI layer, and thus the atoms migration between the gold electrodes was blocked by the PI layer (since it is almost impossible for the atoms penetrate through PI interior to reach the faced electrode), see Figure S11 (Supporting Information) for detailed information. In this case, only symmetric *S*-shaped *I*–*V* curves are observed under different bias ranges, and the current jump is never observed, confirming the migration/trapping of the atoms along the PI surface is a critical step for the realization of electrode reconnection.

Although we only report the technique to in situ reconnect the electrodes by using the O₂ plasma etched PI to trap the electromigrated Au atoms, our strategy, in principle, can be used to trap the electromigrated Cu or Al atoms beyond Au atoms, since the Cu or Al atoms can react with C–O groups as well to form C–O–Cu or C–O–Al complexes.^[34–36] Additionally, we think that our findings may be rationally translated into benefiting the state-of-the-art chip industry by facilitating the fabrication of silicon-based or single-molecule-based field-effect transistor, see Figure S12 (Supporting Information) for detailed information.

Finally, let us analyze the morphology change in the gap area displayed in the SEM images of Figure 2. A bare gap size of ≈20 nm between the electrodes can be observed before the voltage sweep, as shown in Figure 2g. Nevertheless, we believe that the two electrodes are not completely broken, i.e., they are connected by a thin PI layer underneath the electrodes that cannot be completely removed by the etching process, which is hard to be detected in the SEM image due to the weak secondary electron scattering of PI. When the gold atoms were trapped on the etched PI surface inside the gap, the SEM image shows that the two electrodes are reconnected due to the strong secondary electron scattering of gold atoms (Figure 2i).

3. Conclusion

With the ongoing miniaturization of functional building blocks in microelectronic circuits, the breakdown of electronic circuits may become an awkward problem. However, it faces a great challenge to in situ repair a nanoscale circuit with atomic scale fractured nanogaps by traditional methods. Here, we proposed a method to reconnect nanogapped electrodes over 20 nm gaps on etched PI substrates, no need to locate the position of nanogaps. The in situ healing of the nanoscale circuit is achieved by using the O₂ plasma etched PI substrate to trap migrating metal atoms which progressively fill the nanogap between two metal electrodes. This straightforward technique (*I*–*V* sweeps) with low drive voltage (≈2 V) not only shows an advantage to heal nanoscale circuits in situ which is urgently desired in the chip-related industry but also enables us to adjust multiple conductance states of the in-plane junctions toward realizing an atomic scale switches.

4. Experimental Section

Fabrication of Nanogapped Electrodes on Etched PI: The first type of nanogap was fabricated by EBL. A silicon wafer (or thin spring steel) substrate was immersed in acetone, ethanol, and deionized water for ultrasonic cleaning. After that, a PI layer was spin-coated on top of the

silicon wafer (or spring steel) followed by a heating process to harden it. A layer of positive photoresist (poly(methylmethacrylate), PMMA) with a thickness of approximately 200 nm was spin-coated on the PI layer, followed by a curing process. The designed electrode pattern was obtained using electron beam writing (Sigma 500 and ELPHY Quantum, Zeiss, German). A standard development procedure was applied by immersing the substrate into a development solution, after which the substrate was transferred into isopropanol to stop the development process. After developing, a thin film of gold was deposited on the sample surface *via* ion sputtering, and then the sample was immersed in acetone to remove the redundant PMMA and above metal layer. Finally, part of the PI under the gold electrode was etched by ICP etching to obtain a suspended nano-bridge, where a thin PI film underneath the electrodes cannot be fully removed, see Figure S1 (Supporting Information) for detailed information.

Supporting Information

Supporting Information is available from the Wiley Online Library or from the author.

Acknowledgements

This work was supported by the National Key R&D Program of China (2021YFA1200103), the National Natural Science Foundation of China (22273041, 91950116, 11804170, 12174201), and the Natural Science Foundation of Tianjin (19JCZDJC31000, 19JCQJC60900, 22JCYBJC01310) as well as by the Deutsche Forschungsgemeinschaft under the Plasmochrom project (project ID 406778771).

Conflict of Interest

The authors declare no conflict of interest.

Data Availability Statement

The data that support the findings of this study are available in the supplementary material of this article.

Keywords

metal atom trapping, nanoelectrodes, O₂ plasma etching, self-healing, X-ray photoelectron spectroscopy

Received: August 18, 2023

Revised: October 1, 2023

Published online: November 21, 2023

- [1] M.-Y. Li, S.-K. Su, H.-S. P. Wong, L.-J. J. N. Li, *Nature* **2019**, *567*, 169.
- [2] P. S. Peercy, *Nature* **2000**, *406*, 1023.
- [3] I. A. Blech, E. S. Meieran, *Appl. Phys. Lett.* **1967**, *11*, 263.
- [4] P. B. Ghatge, *Appl. Phys. Lett.* **1967**, *11*, 14.
- [5] M. L. Trouwborst, S. J. van der Molen, B. J. van Wees, *J. Appl. Phys.* **2006**, *99*, 114316.
- [6] D. Xiang, X. Wang, C. Jia, T. Lee, X. Guo, *Chem. Rev.* **2016**, *116*, 4318.
- [7] Y. Liu, K. He, G. Chen, W. R. Leow, X. Chen, *Chem. Rev.* **2017**, *117*, 12893.
- [8] S. Huang, Y. Liu, Y. Zhao, Z. Ren, C. F. Guo, *Adv. Funct. Mater.* **2018**, *29*, 1805924.
- [9] B. Wang, W. Huang, L. Chi, M. Al-Hashimi, T. J. Marks, A. Facchetti, *Chem. Rev.* **2018**, *118*, 5690.

- [10] H. Zhou, W. Qin, Q. Yu, H. Cheng, X. Yu, H. Wu, *Nanomaterials* **2019**, 9, 283.
- [11] T. Cheng, Y. Zhang, W. Y. Lai, W. Huang, *Adv. Mater.* **2015**, 27, 3349.
- [12] D. Wang, Y. Zhang, X. Lu, Z. Ma, C. Xie, Z. Zheng, *Chem. Soc. Rev.* **2018**, 47, 4611.
- [13] Y. Peng, T. Cullis, B. Inkson, *Nano Lett.* **2009**, 9, 91.
- [14] W. Xing, J. Hu, S. C. Kung, K. C. Donovan, W. Yan, R. Wu, R. M. Penner, *Nano Lett.* **2012**, 12, 1729.
- [15] C. Schirm, M. Matt, F. Pauly, J. C. Cuevas, P. Nielaba, E. Scheer, *Nat. Nanotechnol.* **2013**, 8, 645.
- [16] B. Putz, O. Glushko, M. J. Cordill, *Mater. Res. Lett.* **2016**, 4, 43.
- [17] R. J. Barsotti Jr., M. D. Vahey, R. Wartena, Y.-M. Chiang, J. Voldman, F. Stellacci, *Small* **2007**, 3, 488.
- [18] S. Valizadeh, M. Abid, F. Hernández-Ramírez, A. R. Rodríguez, K. Hjort, J. Å. Schweitz, *Nanotechnology* **2007**, 18, 1134.
- [19] O. Ram, *SPIE* **2014**, 8967, 327.
- [20] A. W. Hunt, S. P. Riege, J. A. Prybyla, *Appl. Phys. Lett.* **1997**, 70, 2541.
- [21] S. Zhang, N. van Dijk, S. van der Zwaag, *Acta Metall. Sin.* **2020**, 33, 1167.
- [22] J. M. van Ruitenbeek, A. Alvarez, I. Piñeyro, C. Grahmann, P. Joyez, M. H. Devoret, D. Esteve, C. Urbina, *Rev. Sci. Instrum.* **1996**, 67, 108.
- [23] S. Park, G. Wang, B. Cho, Y. Kim, S. Song, Y. Ji, M.-H. Yoon, T. Lee, *Nat. Nanotechnol.* **2012**, 7, 438.
- [24] R. Liu, J.-J. Bi, Z. Xie, K. Yin, D. Wang, G.-P. Zhang, D. Xiang, C.-K. Wang, Z.-L. Li, *Phys. Rev. Appl.* **2018**, 9, 054023.
- [25] Q. Wang, R. Liu, D. Xiang, M. Sun, Z. Zhao, L. Sun, T. Mei, P. Wu, H. Liu, X. Guo, Z.-L. Li, T. Lee, *ACS Nano* **2016**, 10, 9695.
- [26] C. Xiang, J. Y. Kim, R. M. Penner, *Nano Lett.* **2009**, 9, 2133.
- [27] K. Takiya, Y. Tomoda, W. Kume, S. Ueno, T. Watanabe, J. Shirakashi, *Appl. Surf. Sci.* **2012**, 258, 2029.
- [28] K. Sakai, M. Yagi, M. Ito, J.-I. Shirakashi, *J. Vac. Sci. Technol., B* **2022**, 40, 053202.
- [29] S. Zhang, C. Guo, L. Ni, K. M. Hans, W. Zhang, S. Peng, Z. Zhao, D. C. Guhr, Z. Qi, H. J. N. T. Liu, *Nano Today* **2021**, 39, 101226.
- [30] C. Guo, X. Chen, S.-Y. Ding, D. Mayer, Q. Wang, Z. Zhao, L. Ni, H. Liu, T. Lee, B. Xu, D. Xiang, *ACS Nano* **2018**, 12, 11229.
- [31] E. Kondoh, *Coatings* **2022**, 12, 334.
- [32] M. Wang, T. Wang, O. S. Ojambati, T. J. Duffin, K. Kang, T. Lee, E. Scheer, D. Xiang, C. A. Nijhuis, *Nat. Rev. Chem.* **2022**, 6, 681.
- [33] L. Atanasoska, S. G. Anderson, H. M. Meyer, Z. Lin, J. H. Weaver, *J. Vac. Sci. Technol., A* **1987**, 5, 3325.
- [34] K. Fatyeyeva, A. Dahi, C. Chappay, D. Langevin, J.-M. Valletton, F. Poncin-Epaillard, S. Marais, *RSC Adv.* **2014**, 4, 31036.
- [35] S. Park, Y. C. Kim, K. Choi, H. Chae, J. Suhr, J.-D. Nam, *J. Korean Phys. Soc.* **2017**, 71, 1019.
- [36] J. W. Bartha, P. O. Hahn, F. LeGoues, P. S. Ho, *J. Vac. Sci. Technol., A* **1985**, 3, 1390.
- [37] M. Cen-Puc, A. Schander, M. G. Vargas Gleason, W. Lang, *Polymers* **2021**, 13, 1955.
- [38] K. Usami, T. Ishijima, H. Toyoda, *Thin Solid Films* **2012**, 521, 22.
- [39] T. A. Su, M. Neupane, M. L. Steigerwald, L. Venkataraman, C. Nuckolls, *Nat. Rev. Mater.* **2016**, 1, 16002.
- [40] G. Mitra, V. Delmas, H. Al Sabea, L. Norel, O. Galangau, S. Rigaut, J. Cornil, K. Costuas, E. Scheer, *Nanoscale Adv.* **2022**, 4, 457.
- [41] H. Niu, S. Qi, E. Han, G. Tian, X. Wang, D. Wu, *Mater. Lett.* **2012**, 89, 63.
- [42] D. Ji, L. Jiang, X. Cai, H. Dong, Q. Meng, G. Tian, D. Wu, J. Li, W. Hu, *Org. Electron.* **2013**, 14, 2528.
- [43] P. Kong, H. Tan, T. Lei, J. Wang, W. Yan, R. Wang, E. R. Waclawik, Z. Zheng, Z. Li, *Appl. Catal., B* **2020**, 272, 118964.
- [44] D. Ji, T. Li, Y. Zou, M. Chu, K. Zhou, J. Liu, G. Tian, Z. Zhang, X. Zhang, L. Li, D. Wu, H. Dong, Q. Miao, H. Fuchs, W. Hu, *Nat. Commun.* **2018**, 9, 2339.
- [45] P. Meng, H. Heng, Y. Sun, J. Huang, J. Yang, X. Liu, *Appl. Catal., B* **2018**, 226, 487.
- [46] J. D. Zuber, K. L. Jensen, T. E. Sullivan, *J. Appl. Phys.* **2002**, 91, 9379.
- [47] G. Anderegg, *Pure Appl. Chem.* **1982**, 54, 2693.
- [48] D. Xiang, F. Pyatkov, F. Schröper, A. Offenhäusser, Y. Zhang, D. Mayer, *Chem. - Eur. J.* **2011**, 17, 13166.
- [49] H. Al-Johani, E. Abou-Hamad, A. Jedidi, C. M. Widdifield, J. Viger-Gravel, S. S. Sangar, D. H. Anjum, S. Ould-Chikh, M. N. Hedhili, A. Gurinov, M. J. Kelly, M. El Eter, L. Cavallo, L. Emsley, J.-M. Basset, *Nat. Chem.* **2017**, 9, 890.